Implementing Bayesian Statistics and a Full Systematic Uncertainty Propagation with the Soft X-Ray Tomography Diagnostic on the Madison Symmetric Torus

by

Jay Johnson

A thesis submitted in partial fulfillment of the

requirements for the degree of

Bachelors of Science

(Physics)

at the

University of Wisconsin – Madison

2013

Abstract

The Madison Symmetric Torus uses multiple diagnostics to measure electron temperature (T_e). The soft x-ray (SXR) diagnostic measures T_e from x-ray emission in the plasma and the Thomson Scattering (TS) diagnostic records scattered laser photons to measure T_e and electron density n_e. Bayesian analysis techniques have been developed for the SXR system. A multiple helicity (MH), 1500keV plasma shot has been analyzed within this Bayesian framework to create a distribution of the most likely temperature. This distribution has been combined with a similar distribution of the TS measurement to give a single distribution of the most likely T_e in the plasma. By combining the data from both diagnostics with Bayesian probabilities uncertainty of the model fit is lower than either of the diagnostics alone. A rigorous calculation of systematic uncertainties of the SXR diagnostic is given. The relative systematic uncertainties are shown to be $< 2\%$ of the signal for all 80 of the silicon photodiodes used. The absolute uncertainty is shown to be a nearly constant proportion of the signal over a large range of possible plasma conditions.

Acknowledgements

There are a few people whose work and guidance made this thesis possible. First and foremost, I would like to thank Meghan McGarry. She has put up with my questions for three years and never hesitated to take the time to teach me something new, whether or not it's about physics. My thesis would not have been possible if it weren't for her help and for the work she has done with SXR. I would like to thank my adviser, Dr. Daniel Den Hartog for his insight and patience. It has been my pleasure to work with him over the past three years and I look forward to continue working together over the upcoming months. None of the results of Bayesian analysis would have been possible without the help of Lisa Reusch. She has been an outstanding mentor for the past few months and as we developed IDA. I would also like to thank Hilary Stephens for her help in getting Lisa and me on our feet with IDA project and all her previous work with Bayesian statistics on TS which made our work possible. I would like to thank John Goetz and Paolo Franz for all of their support and physics knowledge that they have passed onto me over the past few years.

Contents

List of Figures

Chapter 1

Introduction

One of the focuses in the study of plasmas is x-ray emission and electron temperature. Understanding the relation between the two of these, and their connection to other plasma characteristics, such as density, plays an important role in the study of plasma confinement and stability. The Madison Symmetric Torus is a magnetic confinement device, in a reversed field pinch (RFP) configuration, that has multiple diagnostics dedicated to measuring x-ray emission and electron temperature. This thesis will focus on two diagnostics that independently measure electron temperature, T_e, the soft x-ray (SXR) diagnostic, and the Thomson Scattering (TS) diagnostic. These two diagnostics provide independent measurements of T_e. A continuing problem in understanding how plasmas behave is the amount of uncertainty in each of these measurements, which can sometimes be as substantial as 15-20% of the total signal. Efforts are made to reduce these errors by combining the data within a single framework.

1.1 Thesis Overview

In this thesis, data from the SXR and TS diagnostic are combined using the integrated data analysis (IDA) technique, to give a single, most likely temperature

profile and a most likely core temperature. IDA implements Bayesian statistics to make use of all the available information from each diagnostic. This is shown to decrease uncertainty of the model fit. Chapter 1 gives an introduction to the SXR and TS diagnostics. It describes the importance of x-ray emission and the double-foil technique for T_e measurements. It also gives a brief overview of the TS measurement used on MST.

Chapter 2 gives an overview of Bayesian Probability Theory and its benefits. It describes the application of Bayesian theory to the SXR diagnostic and gives the result of combining the SXR and TS in a Bayesian framework. Finally, this Chapter elaborates on some of the challenges and limitations encountered while implementing IDA.

Chapter 3 gives a rigorous error propagation for the SXR diagnostic. The systematic uncertainty is shown to be slightly smaller than previously assumed. Although the total uncertainty is dominated by random noise from the differential amplifiers, this analysis offers a confirmation of the scale of the estimated systematic error. Chapter 4 summarizes the results of the thesis and describes further development options of IDA.

1.2 Soft X-Ray Emission

A major contribution to x-ray emission in MST comes from free-free bremsstrahlung radiation. When an electron passes through the field of an ion, it is accelerated and emits bremsstrahlung radiation as x-rays. Two other major sources of x-ray emission include line radiation, when an excited electron decays into lower levels, and recombination radiation, when an ion recaptures an electron into a bound quantum state.

Although line radiation and recombination steps can contribute a great deal of x-rays, by filtering the light through beryllium (Be), their contributions to the total x-ray emission can be minimized. Filter bands can be chosen to avoid known radiation lines and as long as the recombination steps also are outside the filter bands then the recombination radiation contribution cancels out in the temperature calculation [1]. After accounting for these other contributions, the x-ray emission can be considered a function of only plasma density, temperature, and effective atomic mass.

The SXR diagnostic on MST uses this filtering technique to study bremsstrahlung radiation. The measurement of these X-rays can give important information about the temperature and the magnetic structure of the plasma. Electrons will follow the magnetic field lines in a sufficiently hot plasma, so, X-ray emission from these electrons map to the magnetic structure of the plasma. When the magnetic field lines wrap around the torus and reconnect with themselves it forms a magnetic *flux surface*. The temperature and density equilibrate along these magnetic field lines much faster than across magnetic field lines, so to first order, flux surfaces are surfaces of constant temperature and density [1]. Figure 1.1 shows the magnetic topology for an example flux surface and a cross section of the tomographic reconstruction of x-ray emission. Figure 1.2 shows an example flux surface mapping and the line-of-sight for a SXR chord.

1.3 The Double Foil Direct-Brightness Method

There are a couple of different ways that the SXR diagnostic can measure temperature. The first is a tomographic reconstruction. This method can give great 2D representation of the plasma temperature but it is very sensitive to small variations

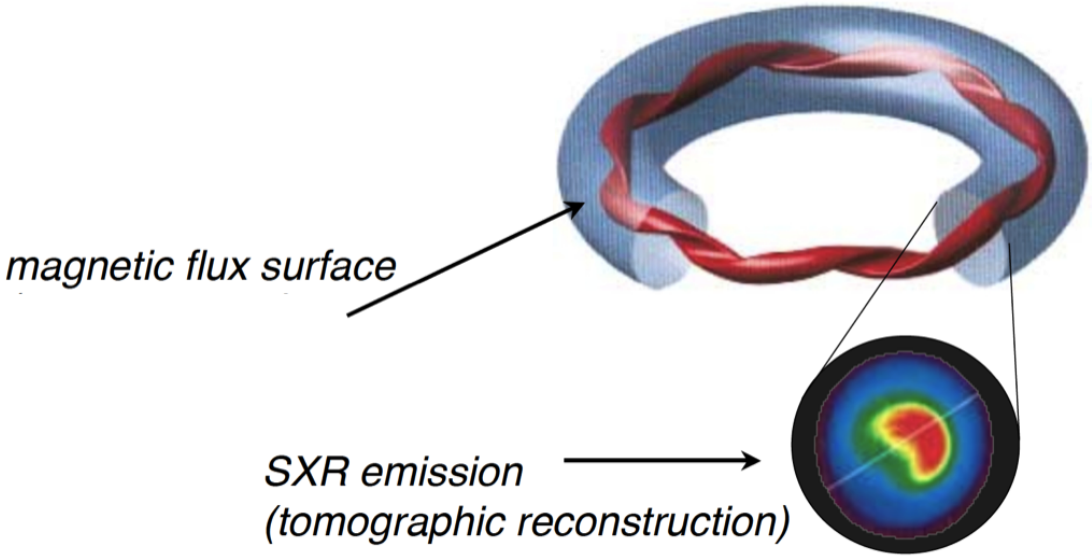

Figure 1.1: The magnetic topology of an example flux surface (particularly the m=1, n=7 magnetic mode) and a cross section of the reconstructed emissivity. (Image courtesy of McGarry [1]).

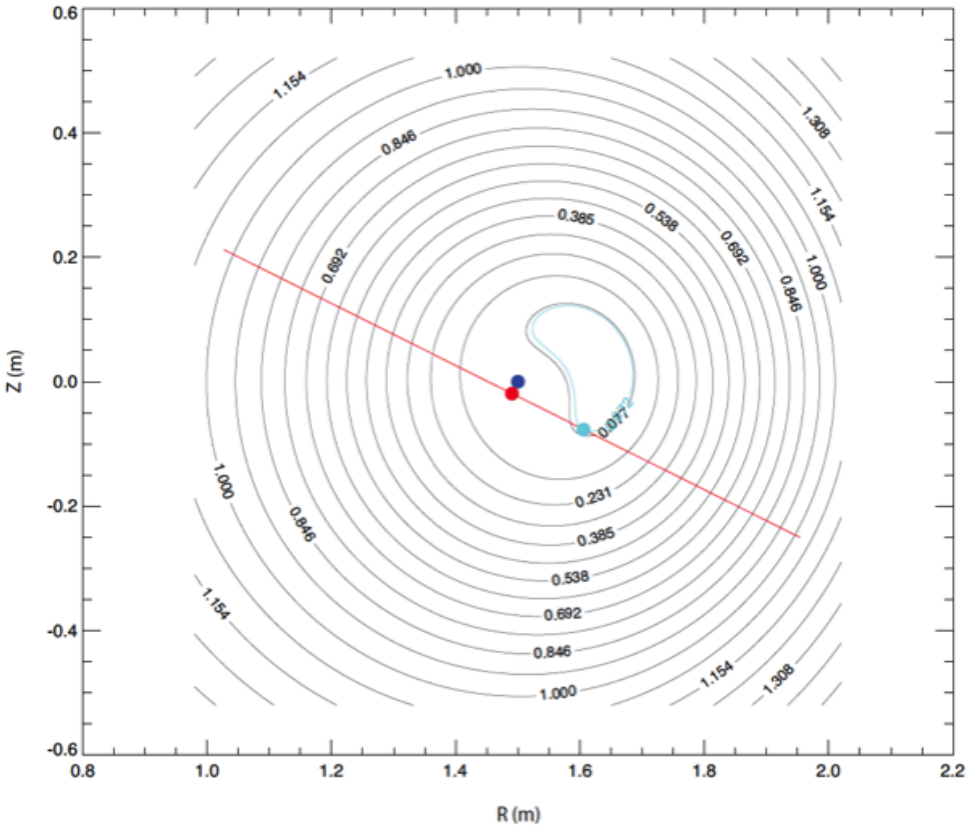

Figure 1.2: An example of the flux surfaces for shot with a magnetic structure at 18° P. The blue dot is the geometric center. The red line is chord 4 from SXR-C. The red dot is the location along the chord that is closest to the geometric axis. The cyan line and dot represent the the innermost flux surface that the chord intersects. The SXR will measure the temperature of this flux surface with the direct-brightness T_e method. (Image courtesy of M. McGarry [1]).

in measured brightness. The direct-brightness method (DB) is the other means to measure temperature and is how the temperature measurements were made for the remainder of this thesis.

In a pure bremsstrahlung plasma, the electrons of a single temperature T_e are not all at the same energy. Instead, there is a distribution over a wide range of energies, given by the Maxwell-Boltzman distribution. The Be acts as a high-pass filter for the photons with sufficient energy. Silicon (Si) photodiodes absorb the x-rays that pass the filters and converts them into a current that can be measured. The currents produced by the photodiodes are very small and need to be amplified by differential amplifiers before they can be digitized and recorded. For a plasma with SXR emission $\varepsilon(E)$, passing through a filter with transmission function $T(E, Be)$, and absorbed by diode with absorption function $A(E)$, the measured brightness is the line-integrated emissivity over the desired energy range, along the line-of-sight of the diode (l).

$$f(l) = \int_L \int_E T(E, Be)\, A(E)\varepsilon(E)\, dl\, dE \tag{1.1}$$

Pairs of diodes are aligned close together, so that they share a line-of-sight and therefore, the same line-integral, but they view the plasma through different thickness filters. Because density and effective atomic mass, Z_{eff}, are not functions of energy, the ratio of the measured emissivities is only dependent on electron temperature [3]. The ratio of two emissivities, ε_1, ε_2, that were filtered with two different thickness filters, is defined by:

$$R = \frac{f_1}{f_2} = \frac{\int_l \varepsilon_1\, dl}{\int_l \varepsilon_2\, dl} \tag{1.2}$$

Temperature is not a line-integrated quantity and therefore cannot be de-convolved from a ratio calculation to give temperatures at specific intervals in the line-of-sight. Instead, it is assumed to be the hottest temperature along the line of sight. This corresponds to the temperature of the innermost flux surface that the line-of-sight intersects.

The SXR system has 4 different probes at the same toroidal location on MST (at 90° T) but varying poloidal locations. Each probe has 20 silicon photodiodes aligned in pairs with one viewing the plasma through a thick ($\sim 800\mu$m) Be filter and the other through a thin ($\sim 400\mu$m) filter. This gives a total of 80 unique emissivity measurements and 40 unique lines-of-sight (see figure 1.3) for temperature measurements.

1.4 Thomson Scattering T_e Measurement

The other temperature measurement on MST comes from the Thomson Scattering (TS) diagnostic. Photons incident on an free, charged particle will be absorbed and another, separate photon will be emitted. The energy of the emitted photon is dependent on the wavevector of the incident photon and the velocity of the absorbing electron. The scattering direction of a single photon is determined by this wave vector and velocity. If many photons with the same polarization and energy are incident on a volume, the intensity of the scattered light is proportional to $sin^2(\chi)$, where χ is the angle between the scattered photon trajectories and the electric field of the incident photons [4].

The TS diagnostic is a multi-point laser system that uses two independently triggered Nd:YAG lasers and a 15 m remote-controlled beam line to generate the incident photons [5]. The scattered photons are collected by 21 different polychrometers with

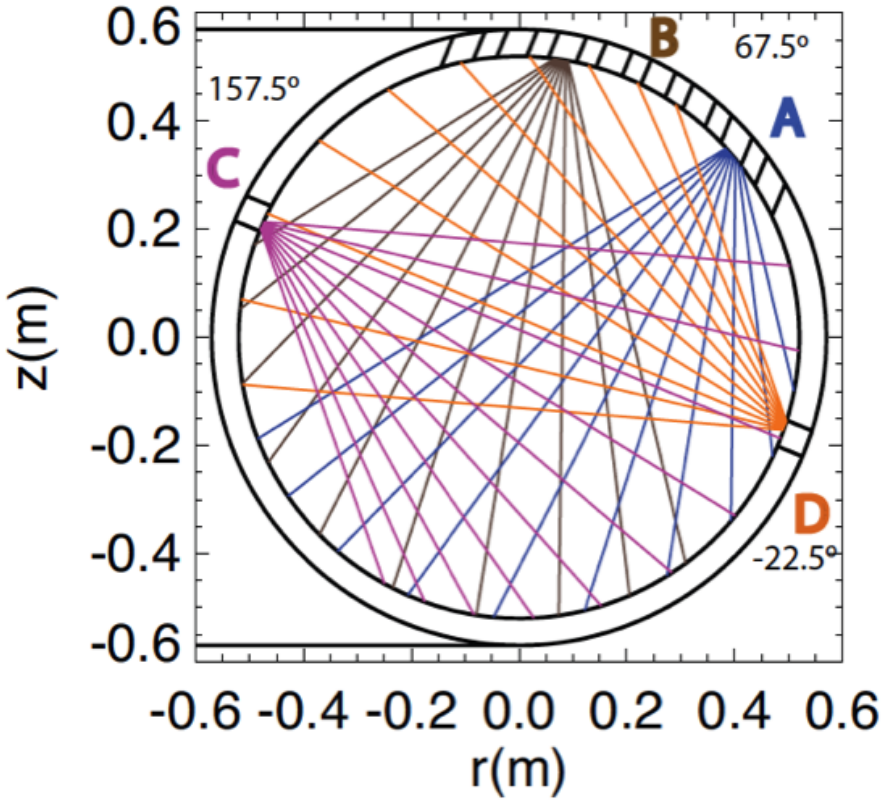

Figure 1.3: A cross section of MST showing the 10 lines-of-sight for each SXR probe. (Image courtesy of M. McGarry [1]).

avalanche photodiode modules. The 21 polychrometers each provide spatially unique temperature and density measurements for the plasma, at 222° T. The 21 TS points form a vertical line through the bottom half of the MST vessel as seen in figure (1.4).

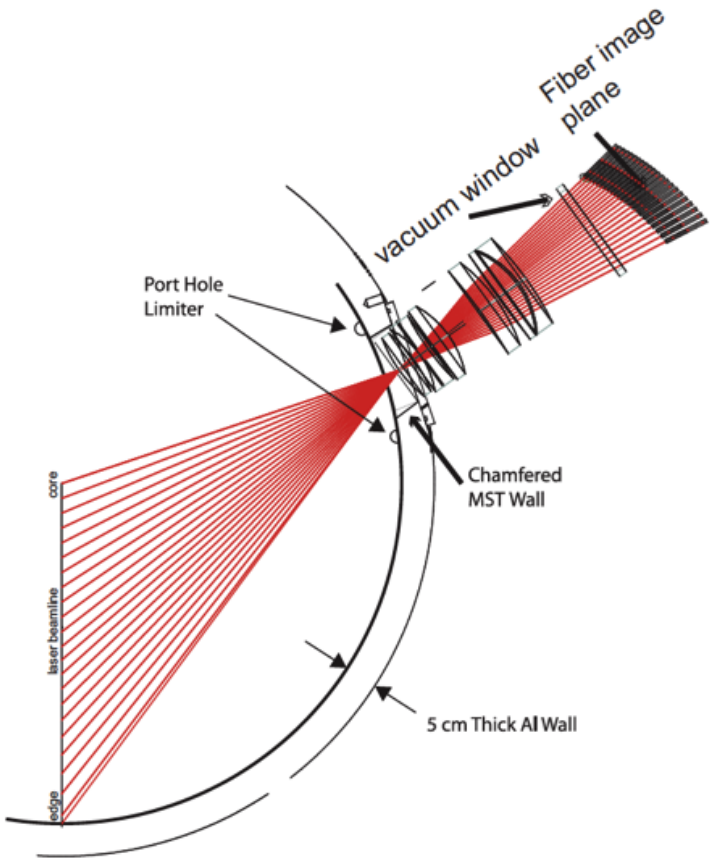

Figure 1.4: The schematic of the TS field of view. Photons scattered from 21 spatial points between the plasma core and MST are collected at the image plane. Diagram courtesy of Rob O'Connell.

Chapter 2

Integrated Data Analysis

The first step to combining data from separate diagnostics is expressing the measurements of each diagnostic in terms of Bayesian probabilities. The TS data has already been put into a Bayesian framework [4, 6]. In this thesis, emissivity data from the SXR system of a multiple helicity (MH) plasma with core temperature of $\sim 1500eV$ will be analyzed using Bayesian probabilities. The SXR data is combined with the TS data and a probability distribution function (PDF) of electron temperature is found. The following section gives a brief introduction to Bayesian probabilities, describes some benefits and drawbacks to Bayesian methods, and presents the work that has been done so far to integrate the TS and SXR measurements into a single estimate of T_e. A complete introduction of Bayesian probability theory can be found in D.S. Sivia's book "Data Analysis: A Bayesian Tutorial" [7].

2.1 Bayesian Statistics

The traditional approach to statistics focuses on the frequency of observing some data, given some hypothesis about its behavior. This method, often called 'frequentist statistics', assumes that the data observed is random, can take a probability between

0 and 1, and that the hypothesis is fixed, it is either true or false. Bayesian statistics takes the opposite approach: the data is fixed, either true or false, and the hypothesis is random, with an associated PDF. A very important feature of Bayesian theory is that it can take into account all relevant background information and any measurement uncertainties.

The following expression is read "The probability that a specific value of X is true given Y is true and any background information, I"

$$P(X|Y,I) \tag{2.1}$$

Starting with two rules from probability theory we will be able to derive the basics of Bayesian probability theory:
The product rule (the probability that X and Y are both true):

$$P(X,Y|I) = P(X|Y,I)P(Y|I) = P(Y|X,I)P(X|I) \tag{2.2}$$

and the addition rule:

$$P(X|I) + P(\bar{X}|I) = 1 \tag{2.3}$$

($\bar{X}$ means that "X is not true"). The addition rule just states that probability of getting X and the probability of *not* getting X must add to 1.

Rearranging Equation (2.2) gives Bayes Theorem:

$$P(X|I) = \frac{P(Y|X,I)P(X,I)}{P(X|Y,I)} \tag{2.4}$$

The main goal of Bayesian analysis is to find the probability that a given parameter or quantity, X, is true based on the data measured, d, any uncertainties , σ, (systematic or statistical), and relevant background information, I. Background information can be as simple as "temperature cannot be negative" to some more substantial knowledge about the particular system being studied. The probability of X being true, known as the posterior probability (or just posterior), $P(X|d, \sigma, I)$, is almost always very difficult to directly calculate. Using Equation (2.4) it can be found with three quantities that are generally much easier to calculate.

$$P(X|d, \sigma, I) = \frac{P(d|X, \sigma, I)P(X|I)}{P(d|I)} \tag{2.5}$$

Equation (2.5) consists of three parts: the PDF or likelihood, $P(d|X, \sigma, I)$, the prior, $P(X, I)$, and the evidence or normalization, $P(d|I)$. The likelihood is the probability of measuring the data, d, given a certain value of X. The prior is the probability of measuring X given the background information. The prior usually can be assumed to be a constant probability if the quantity X is within the ranges of the instruments used to measure it [4]. The evidence is a normalization factor that ensures a total probability of 1.

One immediate benefit from this framework is marginalization, the ability to remove *nuisance parameters* and focus only on the parameters of interest, without losing any information. Nuisance parameters can be parameters that enter the analysis but are not particularily interesting, such as background signals, or even parameters from measurements that are difficult to calibrate. An example of marginalization with the SXR diagnostic can be found in § 2.4. A derivation of the marginalization equation

can be found in [7] and the result is:

$$P(X|I) = \int_{-\infty}^{+\infty} P(X, Y|I) dY \tag{2.6}$$

The PDF, $P(X|I)$, still contains all of the information in $P(X, Y|I)$, but the dependence on Y has been removed by considering all possible values of Y. The power of marginalization becomes even more apparent as more and more parameters are being optimized; It provides a simple way to visualize the distribution of a single one variable or the interdependence of two variables using a contour plot.

2.2 Pros and Cons of Bayesian Statistics

There are many advantages to analyzing MST data in a Bayesian framework. The first is that it provides a means of combining the information from many different diagnostics in a rigorous manner. If a PDF can be generated for a parameter, X, using one diagnostic, and another can be generated for the same parameter using another diagnostic, then the information from both can be combined in a single distribution. Another advantage of Bayesian statistics is that it can give a clear method for model selection. The probability of getting the data, given a parameter X, $P(d|X, \sigma, I)$, can be a measure of the accuracy of a model. To compare two different models, the total probability of getting the data, (d), with a model, (M_1), is written as, $P(d|M_1)$. This can be compared to the total probability of getting the data with a different model, (M_2), $P(d|M_2)$ [8]. A probability $P(d|M)$, is the integral over all parameters of a given model and is a concrete tool to discriminate between models.

There are some notable drawbacks to implementing Bayesian statistics. The first

is that computation time can quickly become an issues if there are many parameters in the model and a 'brute force' method is used. If a full PDF for a model with parameters, X_i, $P(X_i|d, \sigma, I)$, is created, then it is necessary to evaluate the model for each combination of parameters. As the parameter space is discretized more finely, the amount of computing time needed scales linearly with the number of iterations. Problems can arise very quickly if there are many parameters or there is a need to distinguish very subtle differences in parameter value. One way to overcome this is by implementing a search algorithm, such as a Markov Chain Monte Carlo (MCMC) technique. These algorithms can take much more time to initially design than a straightforward, full calculation, but can dramatically increase computing speed. Furthermore, decreasing computation time, thereby increases the ability to analyze more and more parameters. Another drawback is that it not always straightforward to create PDFs that can be combined. This is still a problem with the combination of TS and SXR data that is discussed in § 2.5.

2.3 Applying IDA to SXR

The distribution, $P(d|X, \sigma, I)$, from the right hand side of Equation (2.5), is calculated using a model for SXR emissivity and the known uncertainties. The model generates the emissivity at all points in the plasma and integrates the detector lines of sight to create a simulated brightness, for each possible combination of different parameters. The uncertainty of the measured brightness, σ, is a combination of systematic uncertainty in the geometry of the diagnostic and random error due to electronic noise from the differential amplifiers. For each combination of model parameters, the probability of getting the data is found by taking σ to be the variance of a Gaussian

distribution, centered at the line integrated brightness generated by the model. A distribution is made for each parameter of the model, at each diode location. The n-dimensional matrix of possible combinations of n parameters, for each diode, is referred to as the *parameter space*. The parameter space represents all possible outcomes of the model, within the intervals and coarseness restrictions set for each parameter. The parameter space does not need to be regenerated for each shot analyzed. A new one is necessary only when the parameters are changed or a different model is chosen.

2.3.1 The Simplified SXR Model

The model predicts only the emission from bremsstrahlung radiation in a hydrogen plasma where there are no temperature or magnetic. The electron temperature and density are assumed to be axisymmetric and monotonically decreasing from the core out to the edge in the form of power-law functions:

$$T_e(r) = T_e(0)(1 - (r/a)^{\alpha})^{\beta} \tag{2.7}$$

$$n_e(r) = n_e(0)(1 - (r/a)^{\gamma}) \tag{2.8}$$

where r/a is the radius normalized to the minor radius of MST and α, β, and γ are the power-law exponents describing the profile shapes. In many multiple helicity (MH) plasmas when there are relatively flat T_e and n_e profiles, this model is sufficient. This model is very limited in that it cannot be used if there are temperature or density structures. In the case of when structures are present, a different model is used, described in detail in McGarry [1], The model combines an equilibrium temperature and density (as in Equations (2.7) and (2.8)) with a gaussian shaped temperature

island and a ring shaped density perturbation added on top, described by:

$$T_e(r) = T_e(0)(1-(r/a)^{\alpha})^{\beta} + \Delta T_e e^{-(\delta r_T - r)^2/2\Delta r_T^2} e^{-(\delta\theta-\theta)^2/\Delta\theta^2} \tag{2.9}$$

$$n_e(r) = n_e(0)(1-(r/a)^{\gamma}) + \Delta n_e e^{-(\delta r_n - r)^2/2\Delta r_n^2} \tag{2.10}$$

In Equation (2.9), the Gaussian temperature perturbation has an amplitude ΔT_e above the equilibrium profile. It is centered at the point $(\delta r_T, \delta\theta)$, with a radial width Δr_T, and a poloidal width $\Delta\theta$. The density profile of Equation (2.10) has a perturbation amplitude Δn_e, centered at δr_n, with width Δr_n and is not dependent on poloidal angle [9].

The modeled and measured brightness are described in great detail in [1] and will be briefly outlined here. The simplest model for line-integrated brightness (the measured quantity on MST) for a particular diode assumes SXR emission from bremsstrahlung radiation. The emissivity, ε, is a function of electron temperature profile $T_e(r)$, density profile $n_e(r)$, and the effective atomic number of the plasma, Z_{eff}, at a radius (r):

$$\varepsilon = \int_E dE \left\{ \frac{Z_{eff} n_e^2(r)}{\sqrt{T_e(r)}} e^{-\frac{E}{T_e(r)}} \right\} \tag{2.11}$$

To simulate the brightness seen by each diode, the transmission of the Be filters $T(E, Be)$, the X-ray absorption of the silicon photodiode A(E), and a geometric factor, f_g , defined by the cone of sight of the diode must be incorporated. The geometric factor is defined as:

$$f_g = \frac{A_d A_{ph}}{4\pi d^2} cos^4\gamma \tag{2.12}$$

A_d is the detector area, A_{ph} is the pinhole area, d is the distance from the pinhole plane to the detector plane, and γ is the angle between the line-of-sight and the normal vector of the detector plane [10].

The Be filter and Si transmission are given by the transmission function:

$$T(t, E) = e^{-t\mu(E)} \tag{2.13}$$

for a material of thickness (t) and absorbing coefficient $\mu(E)$ to each material [11]. The absorbing coefficient is defined as:

$$\mu = c \times (\lambda^a) \times (Z^b) \tag{2.14}$$

for material with atomic number Z and X-rays of wavelength λ . The coefficients a, b, c for both beryllium and silicon can be found in Bardet [12].

The measured x-ray emission by the photodiodes, for any location (r), in a pure bremsstrahlung plasma then becomes:

$$\varepsilon_{obs} = \int_E dE f_g T(E, Be) A(E) \left\{ \frac{Z_{eff} n_e^2(r)}{\sqrt{T_e(r)}} e^{-\frac{E}{T_e(r)}} \right\} \tag{2.15}$$

where $A(E)$ is the absorption of the Si diode (or $1 - T_{Si}(t, E)$).

The SXR brightness measured by a silicon diode is a line-integrated measurement along the line-of-sight of that particular diode (l):

$$f(l) = \int_l dl\, \varepsilon \tag{2.16}$$

so that the final measured brightness of each line-of-sight is:

$$f(L) = \int_l \int_E dl\, dE\, f_g T(E, Be) A(E) \left\{ \frac{Z_{eff} n_e^2(r)}{\sqrt{T_e(r)}} e^{-\frac{E}{T_e(r)}} \right\} \tag{2.17}$$

This line-of-sight integral is unique to each of the 80 different viewing chords on the SXR diagnostic, all of which provide unique information about the plasma. Using this model, assuming a known profile for, $n_e(r)$, the most probable brightness is calculated for both the thick and the thin filters. Then, the ratio of these two brightnesses provides the most likely temperature. This temperature distribution is then combined with the TS temperature distribution to give a single distribution for temperature.

2.3.2 Parameter Space Generation

A parameter space was formed by simulating the line-integrated brightnesses for each SXR viewing chord, using the model for Equation (2.17), for a large number of parameter combinations. So far, the only parameters that were varied, for each viewing chord, were the core temperature, $T_e(0)$, and the power-law parameters for the temperature profile, α, and β. The density profile parameters used were an Abel inversion of the line-integrated density [13] , $n_e(0) = 1.13 \cdot 10^{13} cm^{-3}$, and $\gamma = 4.2$. The temperature of the high current PPCD shots being analyzed are, in general, $\sim 1400eV$. So, in order to incorporate all possible variations, the core temperatures in the parameter space were varied from 500eV to 2keV in steps of 6eV, far below resolution of the SXR system. The measurements of α and β from previous plasma shots were analyzed to find a reasonable range. A range from 7 to 12 was chosen for α and 4 to 19 for β. Different alpha and betas were testing to find the model's sensitivity

to small changes in either parameter. No change was noticeable for steps smaller than 0.5, so, both power-law parameters were varied in steps of 0.25 to ensure adequate resolution. In total, the parameter space consisted of 385581 different iterations of the SXR model for each diode.

2.4 Results

Bayesian statistics have been used to analyze a high-current improved confinement (PPCD) plasma shot, number 1130623047 at $t = 20.5$ms. The raw T_e data from SXR is shown in Figures 2.1 and 2.2, and the raw data from TS is shown in Figure 2.3. Both diagnostics measure an approximate core temperature around 1500eV, but, there are sometimes large point-to-point variations and error bars of $\sim \pm 100$eV. The calculated values of alpha and beta from the tomographic inversion were 7.2 and 14.2, respectively.

Figures 2.4 and 2.5 give the posterior probability of most likely electron temperature, $P(T_e(r)|d, \sigma, I)$, from the SXR and TS diagnostics, respectively. Figure 2.6 is the combined posterior distribution for the most likely temperature profile given the data from SXR and TS. The point-to-point variations seen in the raw data are not present in the posterior, and the uncertainty is greatly reduced.

In Figure 2.7, α, β, and spatial location are marginalized to give a distribution for the most likely core temperature, $T_e(0)$, for SXR and TS. The width of the distributions gives a visualization of the relative uncertainty of the two diagnostics. The more spiked TS profile provides a more confident most probable core temperature, slightly hotter than predicted by the SXR data and this will weight the combined distribution in favor of the TS profile. Figure 2.8 is the most likely core temperature

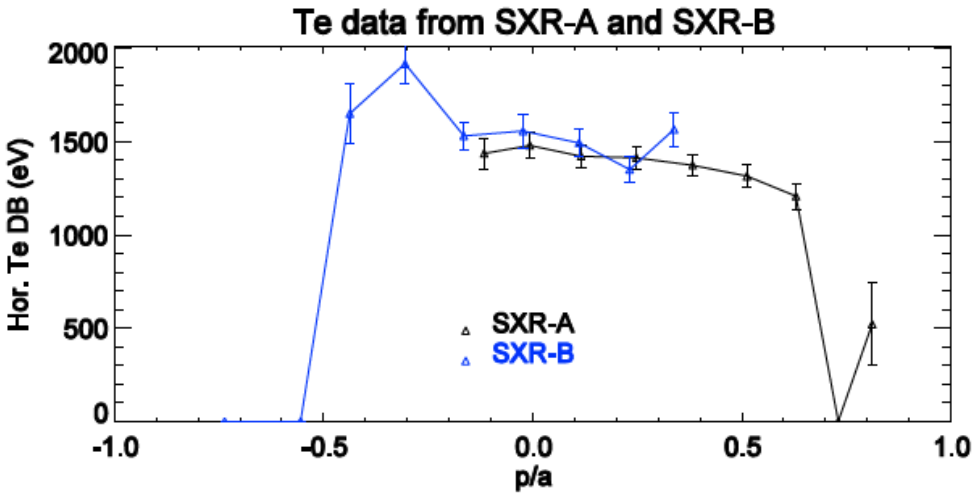

Figure 2.1: Measured direct brightness temperature for SXR-A (black) and SXR-B (blue) from shot number 1130623047 at $t = 20.5$ms.

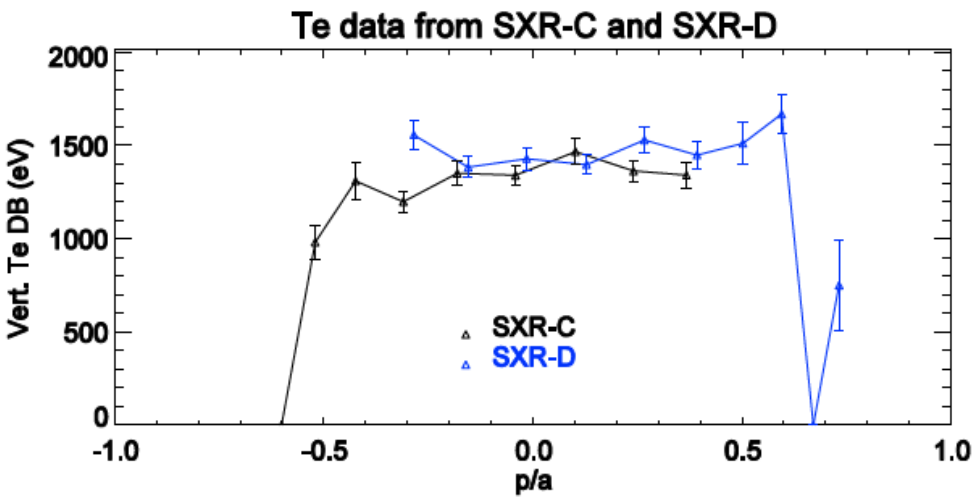

Figure 2.2: Measured direct brightness temperature for SXR-C (black) and SXR-D (blue) from shot number 1130623047 at $t = 20.5$ms.

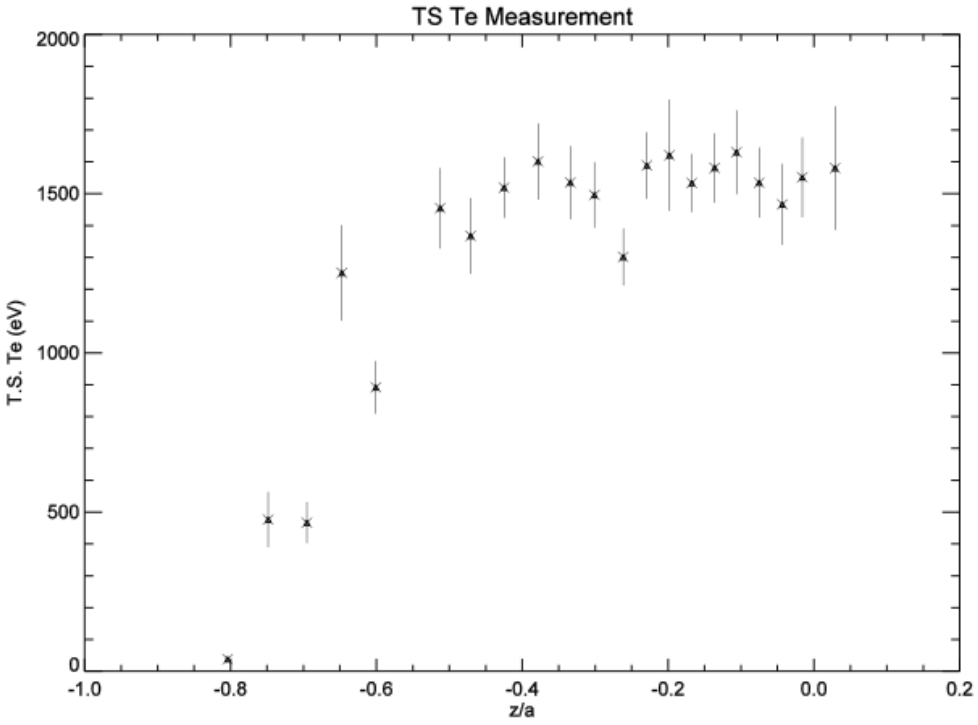

Figure 2.3: The raw temperature data from TS for shot number 1130623047 at $t = 20.5$ms.

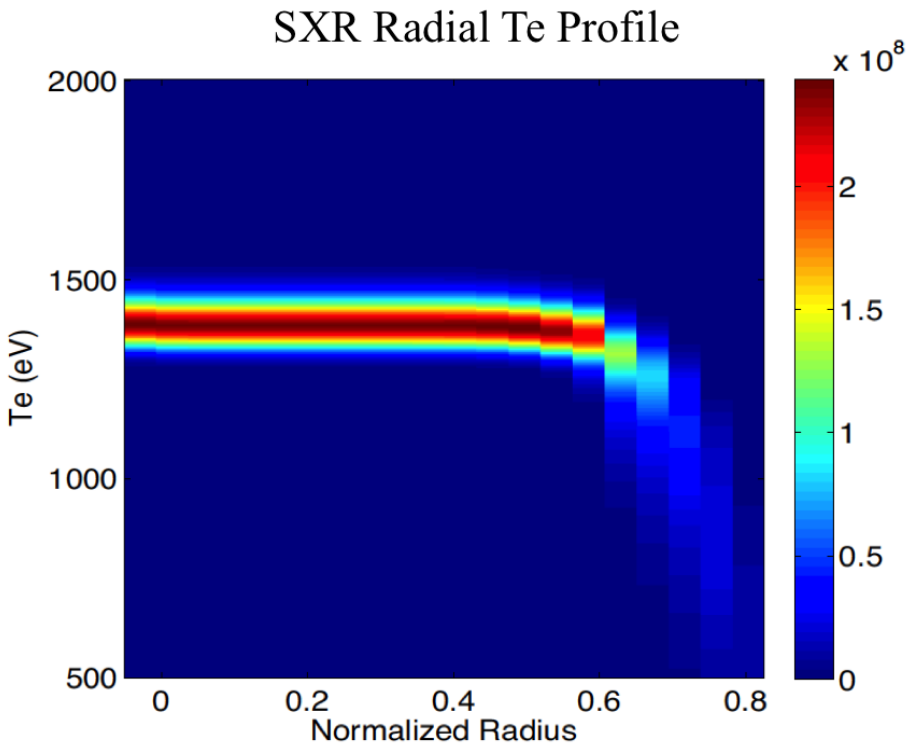

Figure 2.4: The posterior for the radial $T_e(r)$ profile from the SXR data, $P(T_e(r)|d_{SXR}, \sigma, I)$

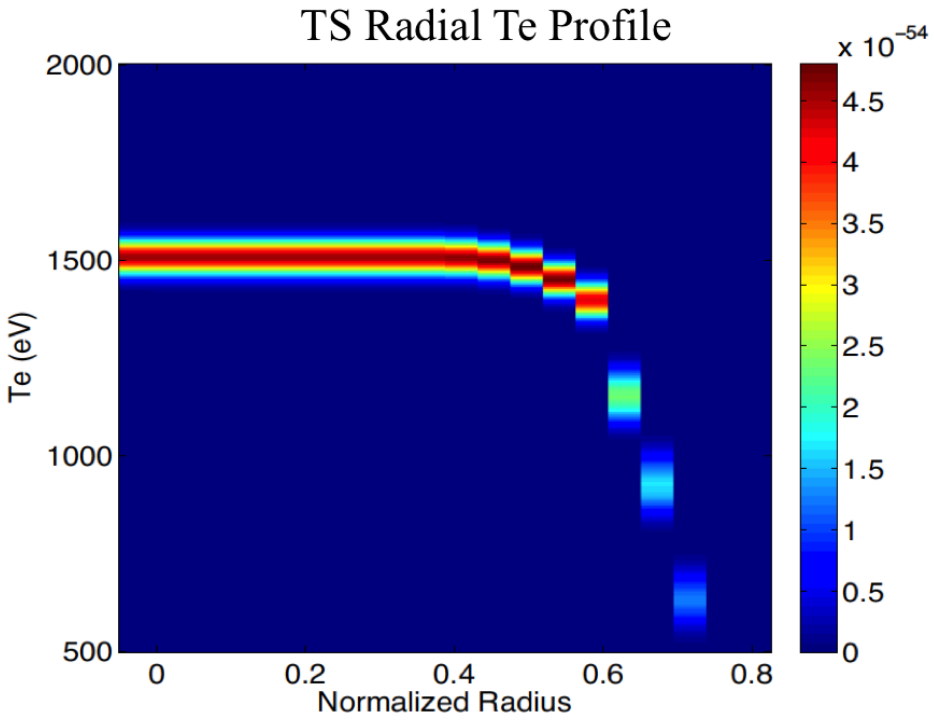

Figure 2.5: The posterior for the radial $T_e(r)$ profile from the TS data, $P(T_e(r)|d_{TS}, \sigma, I)$

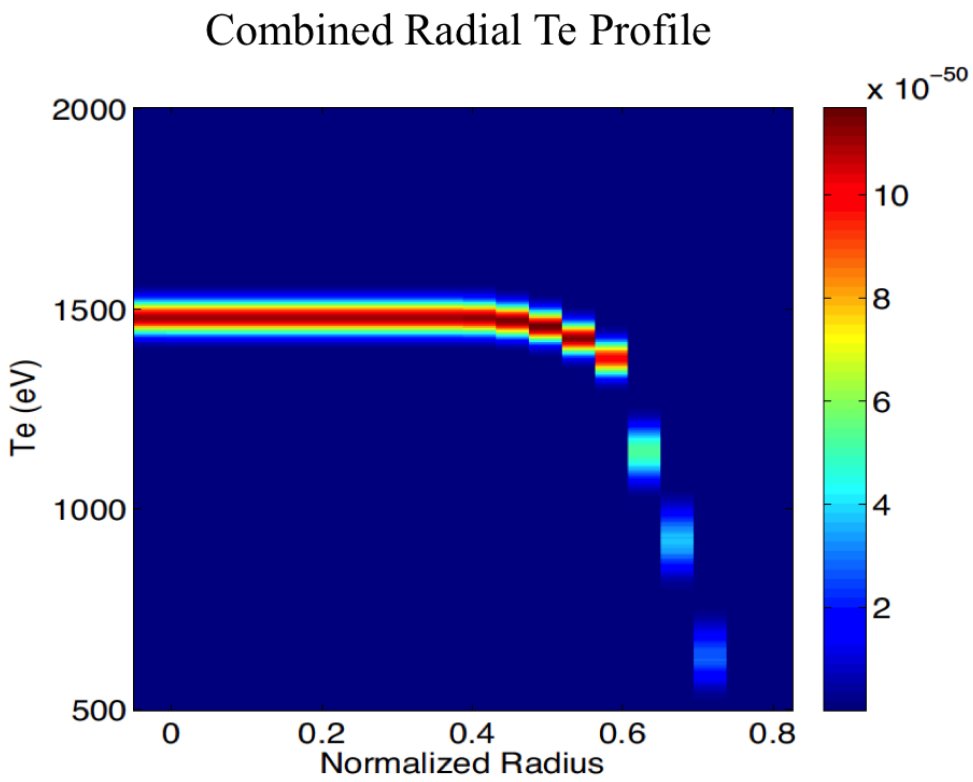

Figure 2.6: The combined posterior for the radial $T_e(r)$ profile from SXR and TS, $P(T_e(r)|d_{SXR}, d_{TS}, \sigma, I)$

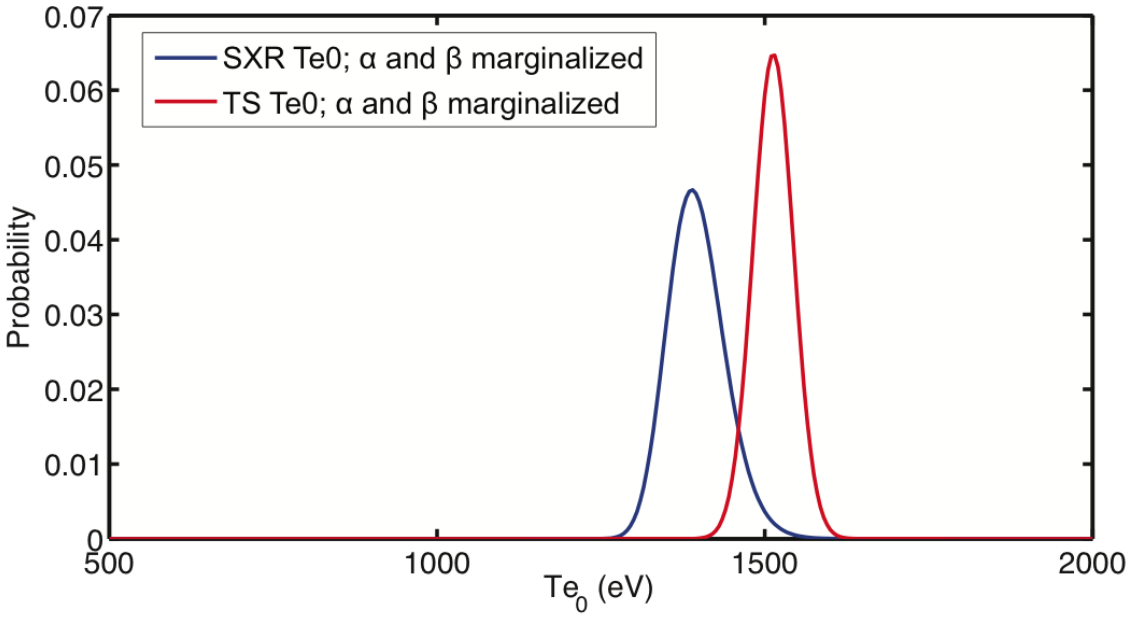

Figure 2.7: Marginalizing α and β from the parameter space leaves a distribution only of core temperature. The broader profile of SXR represents the larger error associated with the SXR system versus the TS diagnostic.

given the SXR and TS data.

The most likely α and β values are found by marginalizing temperature and spatial location. The individual posteriors, $P(\alpha, \beta|d, \sigma, I)$, for SXR and TS are shown in Figures 2.9 and 2.10, respectively. The posterior from SXR in Figure 2.9, is not normalized but that will not change the features, it will only shift the absolute value of the distributions. The PDF from SXR has very broad features, indicating a general inability to resolve α or β. However, in Figure 2.10, the TS distribution has a much sharper peak with most likely values of $\alpha =\sim 7.75$ and $\beta =\sim 13.75$. When combined,

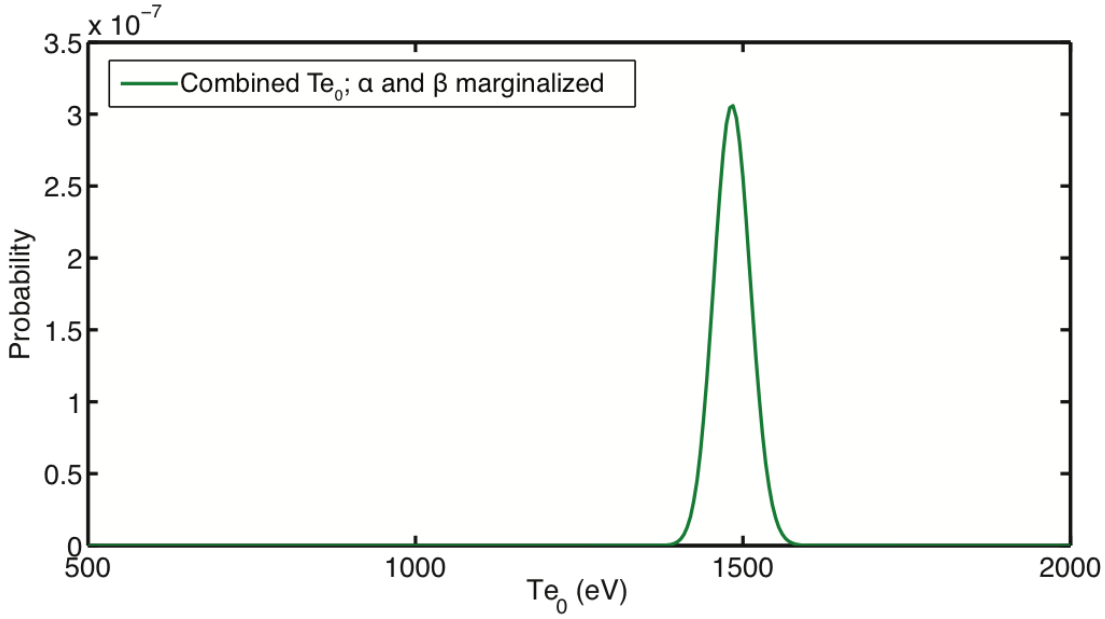

Figure 2.8: The posterior distribution for core temperature, $P(T_e|d_{SXR}, d_{TS}, \sigma, I)$, where α, β and radius, (r), have been marginalized.

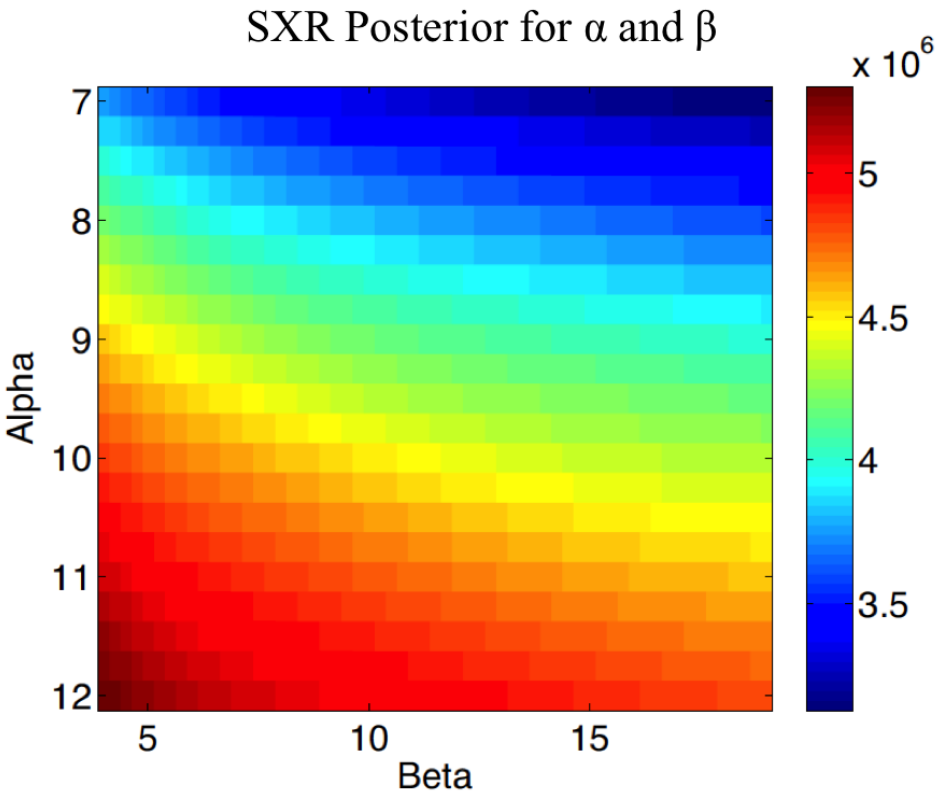

Figure 2.9: The distributions for α and β given the SXR data. $P(\alpha, \beta | d_{SXR}, \sigma, I)$. The darker red areas indicate a more likely outcome. The very broad features emphasize some of the limitations of the SXR system in precisely measuring either α or β. The range for the axis is set using known information about values that α and β can take.

the total distribution is completely dominated by the TS probabilities as seen in Figure 2.11.

2.5 Challenges and Limitations

The first challenge encountered by the IDA project was limits in computation time. The simple SXR temperature model from Equation (2.7), was used to analyze plasmas without any temperature islands,. The density profile was directly taken from

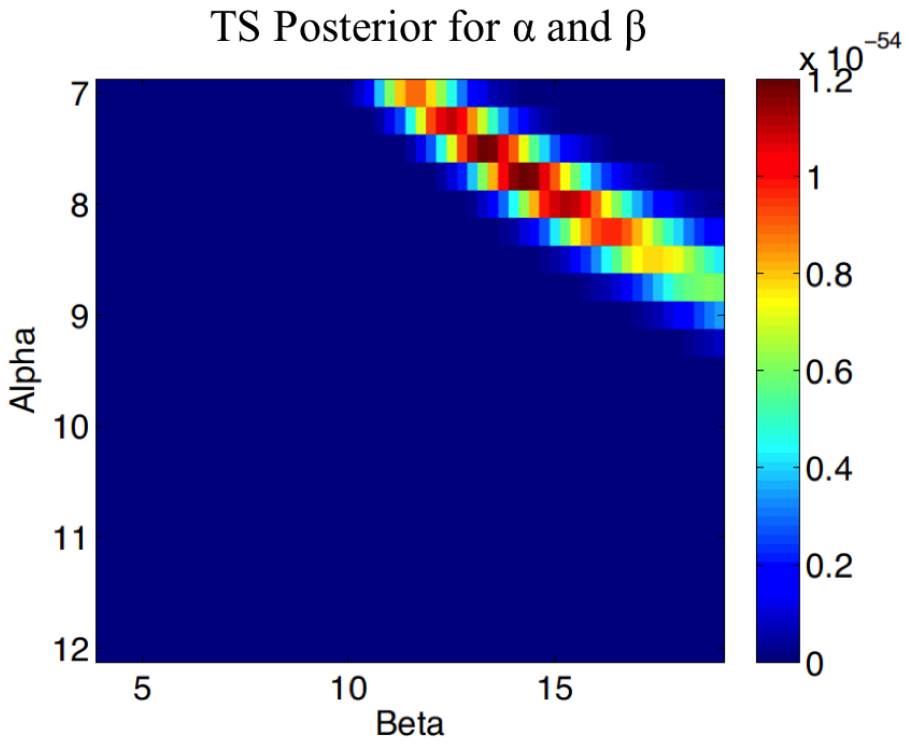

Figure 2.10: The distributions for α and β given the TS data. $P(\alpha, \beta | d_{TS}, \sigma, I)$. The sharp peak is indicates very likely α and β values.

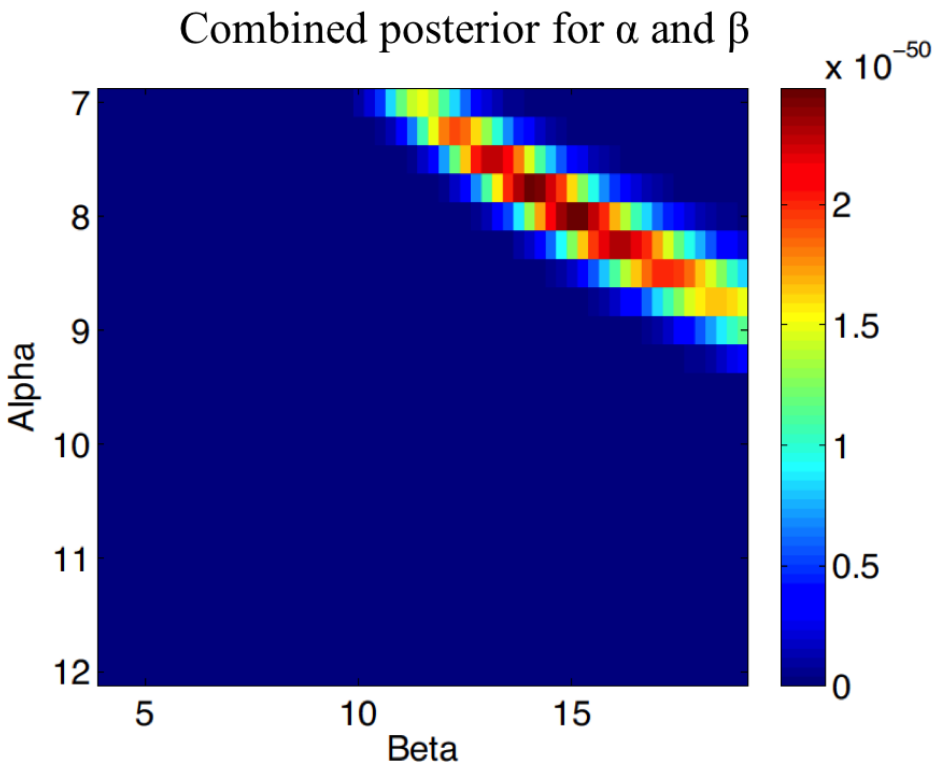

Figure 2.11: The combined posterior distribution of α and β from TS and SXR, $P(\alpha, \beta | d_{TS}, d_{SXR}, \sigma, I)$ The sharp peak in likelihood from TS contributes much more than the broad SXR features.

an Abel inversion of a line integrated n_e [13], so that only three parameters needed to be varied, $T_e(0)$, α, and β. The computation time, for the $\sim 3 \cdot 10^5$ iterations, was on the order of one day using a standard desktop computer. In order to add temperature and density island structures using equations (2.9) and (2.10), 10 more parameters will need to be varied for each of the 80 diodes. If in the future, a model for Z_{eff} would also need to be used, introducing another 6-8 parameters. A conservative calculation of the computation time needed to generate the necessary parameter space to study *only* the full temperature profile, equation (2.9), was on the order of ~ 70 years. Even if the computation time could be significantly reduced, there would still be limited flexibility if more information or parameters were to be added.

Another continuing challenge for the IDA project is finding an effective scheme to spatially relate the temperature measurements from 40 chords on the SXR diagnostic to the 21 Thomson scattering measurements. In order to combine the temperature probability distributions of the two diagnostics, each SXR chord needs to be paired with the TS measurement that views the most similar part of the plasma. Complicated magnetic structures can make this increasingly difficult. Each SXR chord has a temperature probability distribution for a spatial point specified by its impact parameter p and angle ϕ, as defined in [1] and seen in Figure (2.12).

Each TS measurement also has a spatial location in the plasma, but because it is installed at a different toroidal angle, it is not always obvious how to relate it to SXR. In a plasma with no temperature or magnetic structures, the temperature is only dependent on radius and not on poloidal angle. The simplest way to relate the two diagnostics when there are temperature and magnetic structures is by flux

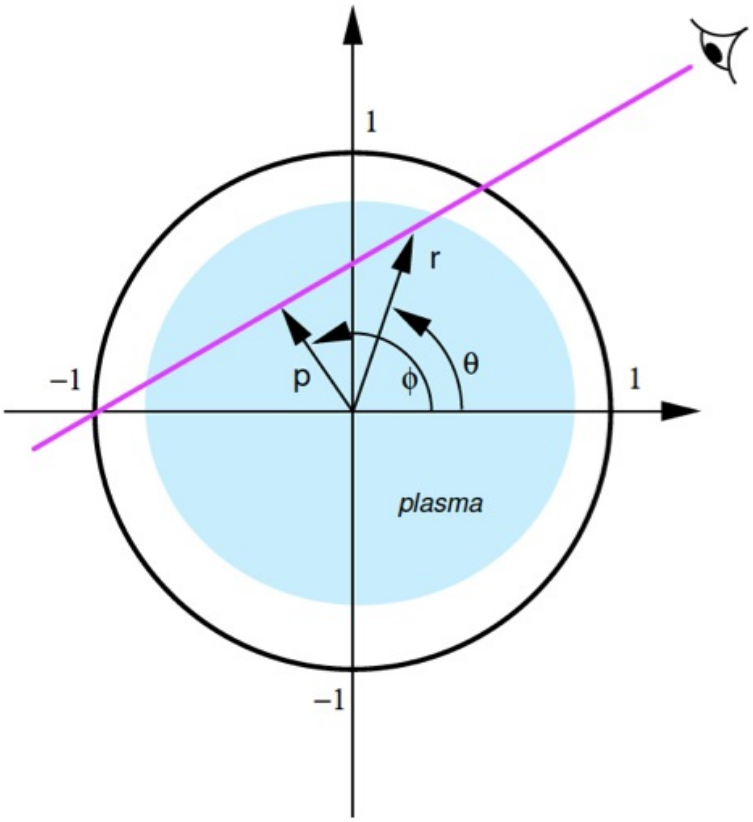

Figure 2.12: The coordinate system used for the SXR system. Each line-of-sight is defined by the impact parameter, p, and angle ϕ.

surface. If the flux surface is known for each SXR chord and for each TS point, then probability distribution of the TS point is multiplied by the nearest SXR distribution in flux surface space. The result is a final temperature distribution as a function of flux surface. Ambiguity arises when emissivity is not monotonically decreasing as flux surface radius increases. This happens when there is a large magnetic island structure offset from the core and is known as a double axis configuration (DAx) plasma. It is then possible to have the SXR emissivity decrease going outward from the core and then increase again near the island and this creates two separate flux surfaces with equal SXR emissivity. The code used to map TS and SXR to flux surface coordinates has not yet been optimized for these DAx plasmas because of this ambiguity.

Chapter 3

Full Uncertainty Propagation for SXR Measurements

The accuracy of Bayesian probabilities is strongly dependent on the uncertainty of the measurements being made. More accurate uncertainties will give a more reliable width to the posterior pdf and ultimately more confidence in the most probable scenario. Therefore, having a thorough understanding of all uncertainties in a measurement is very important when using Bayesian methods. Until now, the systematic uncertainty in the SXR measurement was only roughly approximated as 2% for each diode. In this section, a rigorous analysis of systematic uncertainty in SXR diagnostic is presented. The relative uncertainties for each diode are shown to all be $< 2\%$ using a full error propagation. To find the total systematic uncertainty for a direct brightness measurement, the error for the geometric factor, f_g, the transmission of Be, $T(E, Be)$, and absorption of Si, $A(E)$, from the emissivity equation (2.17) need to be calculated. The other portion of the line-integral,

$$\frac{Z_{eff} n_e^2(r)}{\sqrt{T_e(r)}} e^{-\frac{E}{T_e(r)}},$$

is dependent on plasma conditions and does not add any systematic uncertainties. Because $f_g, T(E, Be)$, and $A(E)$ are all independent variables, the error in the their product can be calculated using the standard variance formula. Including each independent variable, X_i, with variance σ_i^2, the total variance in the quantity, $f(X_i)$ [14] is:

$$\sigma_f^2 = \sum_i \left(\sigma_{X_i} \frac{\partial f}{\partial X_i} \right)^2 \tag{3.1}$$

Defining a function g as:

$$g = f_g * T(E, Be) * A(E) \tag{3.2}$$

The variance of g is:

$$\sigma_g^2 = \sigma_{f_g}^2 \left(\frac{\partial g}{\partial f_g} \right)^2 + \sigma_T^2 \left(\frac{\partial g}{\partial T} \right)^2 + \sigma_A^2 \left(\frac{\partial g}{\partial A} \right)^2 \tag{3.3}$$

Substituting g and σ_g into equation (2.17), the direct brightness measurement becomes:

$$f(L) = \int_L \int_E dE\, dl\, (g \pm \sigma_g)\, \varepsilon(E) \tag{3.4}$$

The total uncertainty in the direct brightness measurement is the line-integral of the product of the uncertainty in g with the portion of the integral dependent on plasma conditions, $\varepsilon(E)$:

$$\sigma_{total} = \int_L \int_E dE\, dl\, \sigma_g\, \varepsilon(E) \tag{3.5}$$

3.1 Error in the Geometric Factor

The geometric factor (f_g), in equation 2.12 accounts for the cone of sight of the diodes. Ideally, the emissivity is a perfect line-integrated quantity through the plasma, but because of the the non-zero area of the diodes and pinhole, this correction factor must be used. The uncertainty in f_g is dependent on uncertainties in the area of the silicon diodes (A_d), the area of the pinhole (A_{ph}), the distance from the pinhole to the diode board (d) and the angle incidence (γ)of the line-of-sight normal to the detector plane.

The length and width of the pinhole were manufactured and independently measured to be within the tolerance of $2.00 \pm 0.01mm$. The standard error of the area is $\sim 0.7\%$. The distance from pinhole to diode board, d, is 25.04mm. It was calculated from three direct measurements of component parts within the probe head, using a $\pm 10\mu m$ micrometer, and has standard error of 0.6%.

The standard variance formula is more complicated when two or more of the variables X_i are not independent quantities. The angle of incident light, γ, is not independent of the distance to the diode board, d. To avoid this problem, the value $cos\,\gamma$ is rewritten using trigonometric identities as:

$$cos\,\gamma = \frac{d}{\sqrt{d^2 + x^2}} \tag{3.6}$$

where x is the distance from the diode to the pinhole in the direction tangent to the diode surface. This substitution is also favorable because the error in the value

x is known well. Each diode was placed and measured to be within of $50\mu m$ of its intended location on the circuit board, independent of the other diodes. This keeps σ_x from compounding as diodes move farther from the center of the board. The width of the pinhole and the width of the diodes are in fact correlated to the distance x, an uncertainty of $10\mu m$ in width can change the value of x by at most $5\mu m$. The error in x, (σ_x) is an order of magnitude larger than the error contribution from the width and can be approximated as simply $50\mu m$. Therefore the total relative error in the geometric factor, f_g varies by diode, depending on angle γ and ranges from about 1.1% to 1.6%.

3.2 Be Uncertainty

Each beryllium filter consists of a stack of individual foils. There are, generally, 5 stacked to make the $421\mu m$ thin filter and 9 or 10 stacked to make the $857\mu m$ thick filter. Each foil has a thickness of $\sim 75-95\mu m$ thick measured to $\pm 1\mu m$ and the total Be filter thickness error σ_{Be}, is calculated as the variance of the individual foil errors (σ_{foil}):

$$\sigma_{Be} = \sqrt{\sum \sigma_{foil}^2} \tag{3.7}$$

The error is then $\sim 0.5\%$ for the thin filter and $\sim 0.4\%$ for the thick filter. This is an improvement on the rough 1% estimate that was assumed in McGarry [1].

The transmission of x-rays through the Be filters is dependent on both the energy of the x-rays (E), the thickness of the filters (t_{Be}), and the absorption coefficient μ_{Be} and related by equation (2.13). X-ray transmission is very sensitive to μ_{Be}, which is affected by impurity contributions in the Be. This dependence is currently being

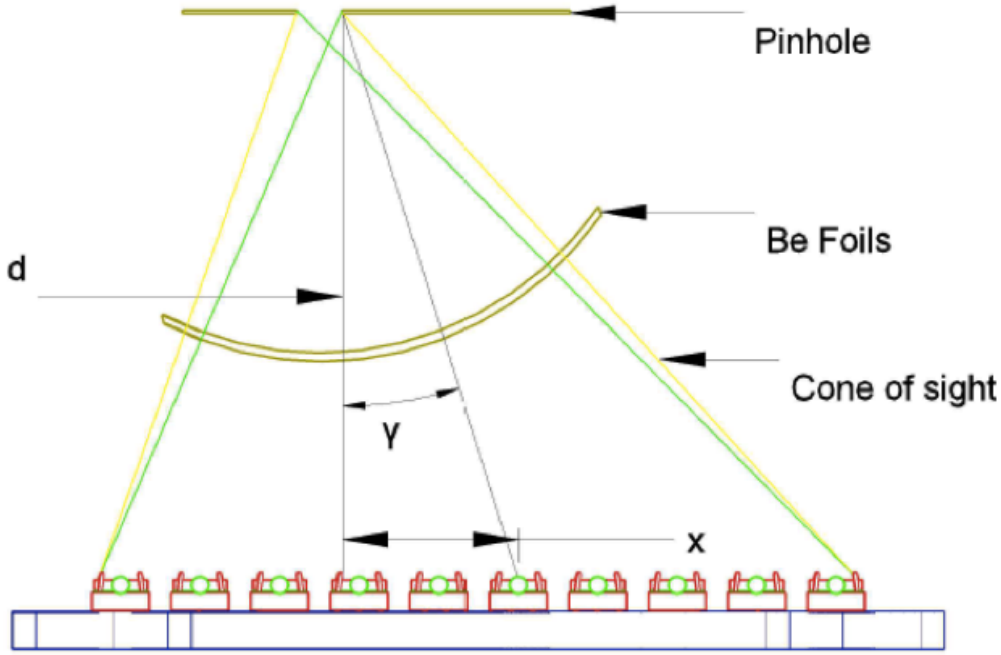

Figure 3.1: A cross section of the probe tip detailing the coordinates x, d, and γ. This view only shows the pinhole, Be foils, line of sight, and diodes.

investigated but is outside the scope of this thesis. The purity is assumed to be 100% for the following calculations.

Because the Be foils are curved so that the effective thickness is constant for all lines-of-sight, the only source of error is in the overall thickness (σ_{Be}) calculated above. Following the standard variance formula, the uncertainty in the transmission function ($T(E)$) is:

$$\sigma_T(E) = T(E)\,\mu_{Be}(E)\,\sigma_{tBe} \tag{3.8}$$

The relative error in the transmission function is actually smaller for the thick filters than for the thin filters.

3.3 Si Uncertainty

For silicon, the absorption of x-rays is dependent on the x-ray energy and the effective thickness of the silicon. The effective thickness (t) will change relative to the angle of incident x-rays (γ) so that the absorption is:

$$A(E) = 1 - e^{t\,\mu_{Si}(E)/cos\,\gamma} \tag{3.9}$$

Using the same substitution for $cos\,\gamma$ as with the geometric factor, equation (3.6), the absorption function becomes a function of the distance from the diode board to the pinhole, d, the distance from the center of the pinhole to the center of each diode, tangent to to the diode board, x, the thickness of the silicon t_{Si}, and photon energy. Following the standard variance formula, a more complicated expression for σ_A can be calculated for each energy and diode. The expression for σ_A has been omitted but

the total percent uncertainty is never more than 0.12%.

3.4 Results of the Uncertainty Calculations

The total uncertainty in the direct brightness measurement, σ_{total}, equation (3.5), was calculated using the uncertainties above and SXR model described earlier, of a plasma with core temperature $T_e(0) = 1525eV$, temperature profile parameters $\alpha = 4.5$ and $\beta = 14$, core density $n_e(0) = 1.13{\cdot}10^{-13}cm^{-3}$ and density profile parameter $\gamma = 4.5$. The relative uncertainties for all diodes are $< 2\%$. The two distinguishing factors for each diode uncertainty are the viewing angle, γ, and the Be filter thickness used. This is apparent in Figures (3.2) and (3.3), where the uncertainties for probes with offset pinholes, (SXR-C and SXR-D), lie directly on top of each other while the uncertainties for probes with center pinholes (SXR-A and SXR-B) also align.

The uncertainties for a range of typical parameter values were calculated over the following ranges to compare the effect of plasma configuration on uncertainty. The ranges for each parameter were, $T_e(0) = 0.5keV - 2keV$, $n_e(0) = 0.5 - 1.13 \cdot 10^{13}cm^{-3}$, $\alpha = 7 - 11$, $\beta = 4 - 19$, and $\gamma = 2 - 9$. The total relative uncertainty did not vary per diode by more than $\sim 0.09\%$ in the two most extreme cases. Figure 3.4 shows the largest change between any two parameter sets for a single set of thin filters with a centered pinhole and a set of thin filters with an offset pinhole. This demonstrates that the absolute error is proportional to the signal levels so that the relative percent error is nearly constant over the measurement range of the SXR diagnostic.

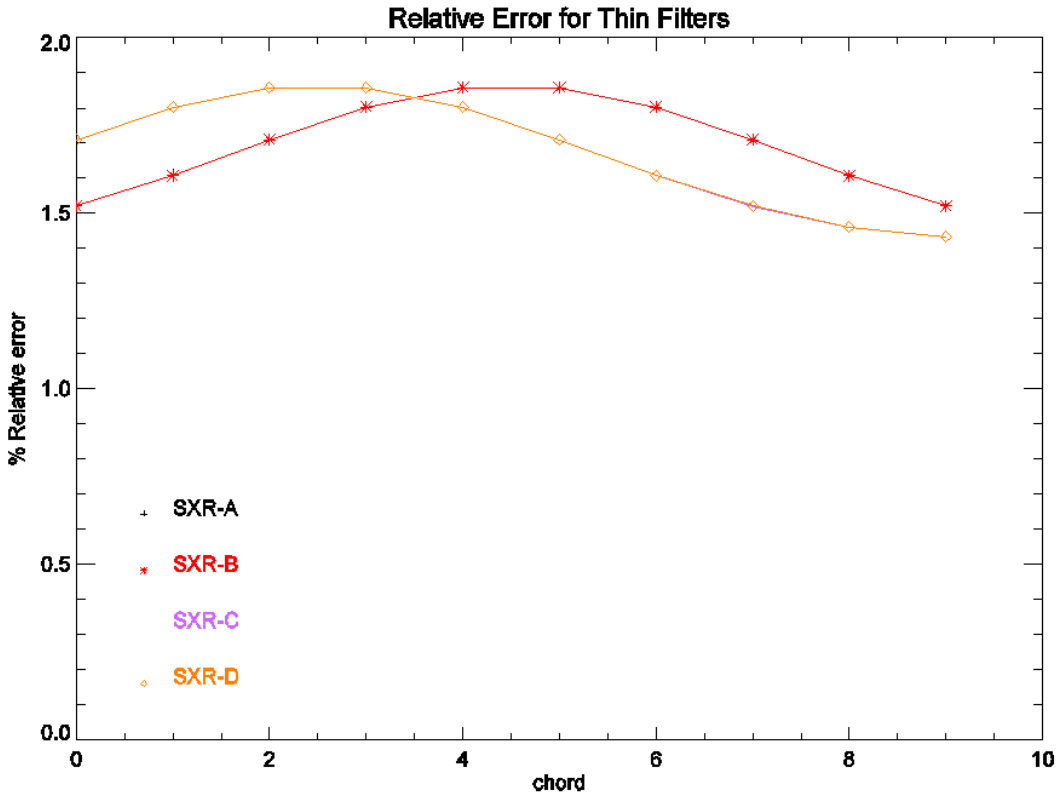

Figure 3.2: Relative error in the direct brightness through the thin filter. The SXR-A and SXR-B profiles lie directly on top of each other and SXR-C and SXR-D profiles lie directly on top of each other.

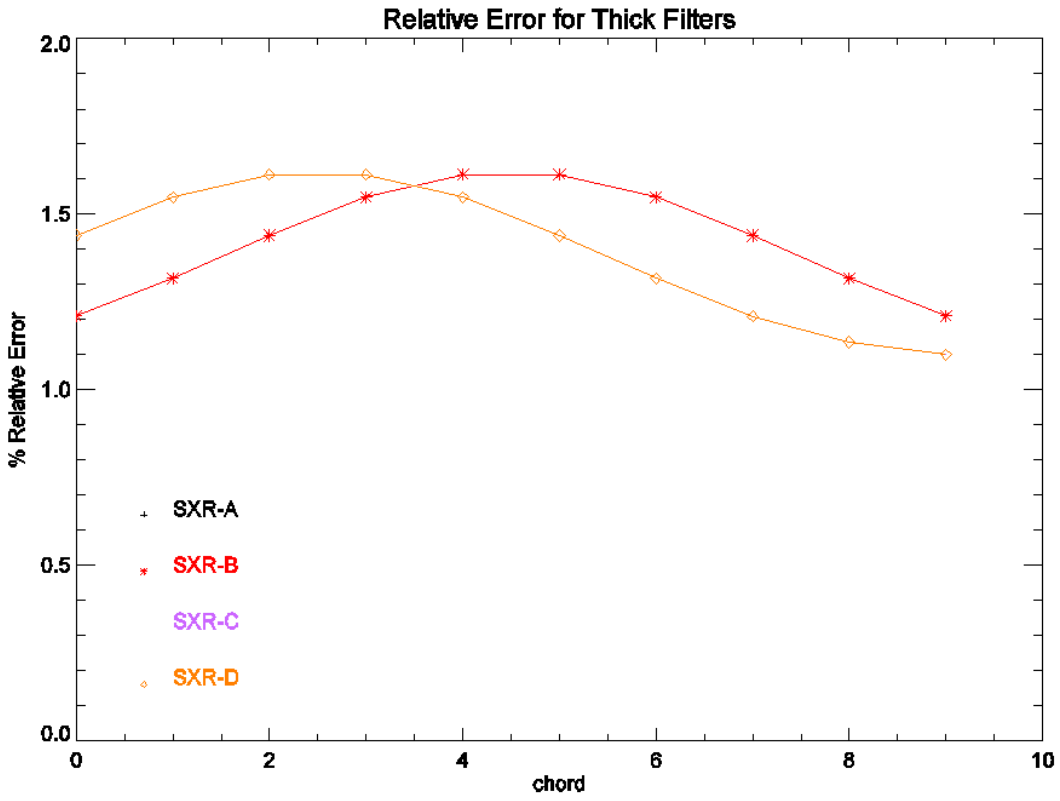

Figure 3.3: Relative error in the direct brightness through the thick filter. The SXR-A and SXR-B profiles lie directly on top of each other and SXR-C and SXR-D profiles lie directly on top of each other.

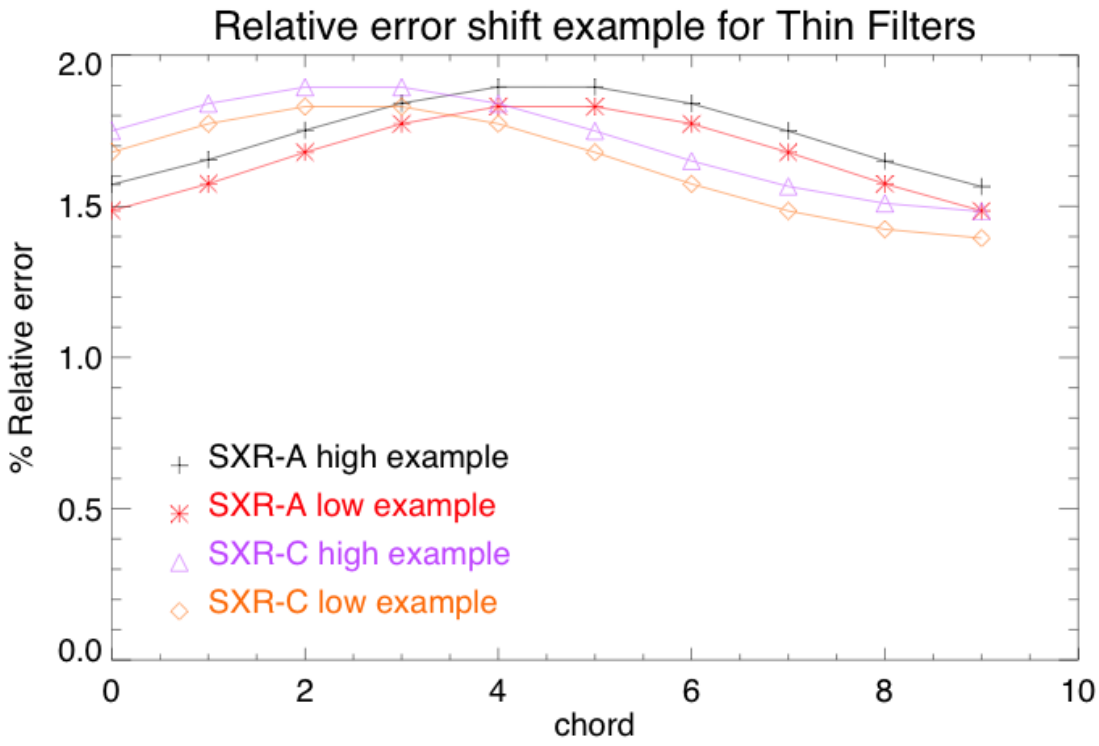

Figure 3.4: The largest difference in relative errors from typical plasma parameters. In the higher profiles, $T_e(0) = 0.5keV$, $n_e(0) = 1.13 \cdot 10^{13} cm^{-3}$, $\alpha = 7$, $\beta = 19$, and $\gamma = 9$. For the lower profiles, $T_e(0) = 2keV$, $n_e(0) = 0.5 \cdot 10^{13} cm^{-3}$, $\alpha = 11$, $\beta = 4$, and $\gamma = 2$.

Chapter 4

Summary and Future Work

Data from the SXR diagnostic has been analyzed within a Bayesian framework to give most-likely distributions for different electron temperature parameters including, $T_e(r)$ and $T_e(0)$, as well as, α, and β from the model of $T_e(r)$. These distributions were combined with distributions previously made with the TS diagnostic to give the posterior distribution, given all of the data from both diagnostics, $P(T_e(r), \alpha, \beta | d_{TS}, d_{SXR}, \sigma, I)$. The posterior provides a clearer understanding of the temperature profile for a MH plasma shot on MST than from the raw data of the two diagnostics separately.

The IDA project will benefit from an optimized mapping of the spatial SXR chords and TS points to the flux surfaces of a DAx configuration plasma. When the magnetic structures become increasingly complicated, flux surfaces offer the simplest method for comparing the measurements of the two toroidally separated diagnostics. With an effective scheme for relating SXR to TS, Bayesian analysis can be used for more plasma configurations.

The other improvement for the IDA project is the implementation of an advanced searching algorithm, such as MCMC. The current method, that creates the entire posterior distribution, does not have the necessary flexibility to incorporate more

parameters to optimize. Future analysis would hopefully include models for Z_{eff}, n_e, and even line or recombination radiation. Currently, computation time and space are strictly limiting factors that would not allow for such an increase in the number of parameters.

The total systematic uncertainty in the SXR diagnostic was calculated to be $< 2\%$ of the total signal for all diodes. It offers a slight improvement on previously assumed uncertainties. The uncertainty was calculated for a wide range of plasma configurations and is shown to vary proportional to signal level, keeping a relatively constant percent error.

The SXR measurement is known to be very sensitive to the purity level of the Be filters. Further analysis of the relation between measured brightness and impurity content is necessary. Once it is better understood, it can be incorporated into uncertainty calculation and included in Bayesian uncertainties of IDA.

References

[1] M.B. McGarry, *Probing the Relationship Between Magnetic and Temperature Structures with Soft X-Rays on the Madison Symmetric Torus*, Ph.D. thesis, University of Wisconsin - Madison, **2013**

[2] F. Bonomo, *Experimental Measurements of Soft X-Ray Emissivity Distribution and Electron Temperature Profile in Reversed Field Pinch Plasmas*, Ph.D. thesis, Universita Delga Studi di Padova, RFX - Italy, **2008**

[3] F.C. Jahoda, E. M. Little, W. E. Quinn, G.A. Sawyer, and T.F. Stratton, "Continuum Radiation in the X-Ray and Visible REgions from a Magnetically Compressed Plasma (Scylla), " *Phys. Rev.*, vol 119, no. 3, p.843, **1960**

[4] H.D. Stephens, *Electron Temperature Structures Associated with Magnetic Tearing Modes in the Madison Symmetric Torus*, Ph.D. thesis, University of Wisconsin - Madison, **2010**

[5] J. A. Reusch, M.T. Borchardt, D. J. Den Hartog, A. F. Falkowski, D. J. Holly, R. O'Connell, and H. D. Stephens. "Multipoint Thomson scattering diagnostic for the Madison Symmetric Torus reversed-field pinch. *Rev. Sci. Instrum.* Vol. 79, 10E733, **2008**

[6] R. O'Connell, DJ. Den Hartog, MT. Borchardt, DJ. Holly, JA. Reusch, HD. Stephens, "Optimizinng a Thomson scattering diagnostic for fast dynamics and high background.", *Rev Sci Instrum.* vol. 79, 10E735 **2008**. http://dx.doi.org/10.1063/1.2957844

[7] D.S. Sivia, *Data Analysis: A Bayesian Tutorial*, Oxford, U.K., Oxford Science Publications, **2006**

[8] R.E. Kass,A. Raftery,"Bayes Factors", *Journal of the American Statistical Association*, Vol.90, No.430. pp.773-795, **1995**

[9] D. Gregoratto, L. Garzotti, P.Innocente, S. Martini, and A. Canton "Behaviour of Electron Density Profiles and Particle Transport Anslysis in the RFX Reversed Field Pinch", *Nucl. Fusion*, vol. 38, no.8, p. 1199, **1998**

[10] P. Franz, L. Marrelli, P. Piovesan, I. Predebon, F. Bonomo, L. Frassinetti, P. Martin, G. Spizzo, B.E. Chapman, D. Craig, and J.S. Sarff, "Tomographic Imaging of Resistive Mode Dynamics in the Madison symmetric Torus Reversed-Field pinch", *Phys Plasmas*, vol. 13, p. 012310, **2006**

[11] T.P. Donaldson, "Theory of Foil-Absorption Techniques for Plasma X-Ray Continuum Measurements." *Plasma Physics*, vol. 20, p. 179, **1978**

[12] R. Bardet. "Coefficients D'Attenuation Massiques Des Rayons X",*Assiciation Euratom-CEA*, Internal Document (DPh-PFC-SIG, EUR-CEA-FC-885),Grenoble, France, **1977**

[13] H.K. Park, "A New Asymmetric Abel-Inversion Method for Plasma Interferometry in Tokamaks," *Plasma Phys. Control. Fusion,* vol. 31, no. 13, p. 2035, **1985**

[14] P.R. Bevington, D.K. Robinson, *Data Reduction and Error Analysis for the Physical Sciences*, New York, NY, McGraw-Hill, **2003**